THE ASTROPHYSICAL JOURNAL, 533:884–889, 2000 April 20
© 2000. The American Astronomical Society. All rights reserved. Printed in U.S.A.

GAMMA-RAY BURST ARRIVAL-TIME LOCALIZATIONS: SIMULTANEOUS OBSERVATIONS BY *ULYSSES*, *PIONEER VENUS ORBITER*, SIGMA, WATCH, AND PHEBUS

K. HURLEY
Space Sciences Laboratory, University of California, Berkeley, Berkeley, CA 94720-7450; khurley@sunspot.ssl.berkeley.edu
J. LAROS
Lunar and Planetary Laboratory, University of Arizona, Tucson, AZ 85715
S. BRANDT, E. E. FENIMORE, R. W. KLEBESADEL, AND J. TERRELL
Los Alamos National Laboratory, Los Alamos, NM 87545
T. CLINE
NASA Goddard Space Flight Center, Code 661, Greenbelt, MD 20771
C. BARAT, M. BOER, AND J.-P. DEZALAY
Centre d' Étude Spatiale des Rayonnements, F-31029 Toulouse Cedex, France
R. SUNYAEV, O. TEREKHOV, A. KUZNETSOV, AND S. SAZONOV
Space Research Institute (IKI), 117810 Moscow, Russia
N. LUND
Danish Space Research Institute, DK-2100 Copenhagen, Denmark
A. CLARET AND J. PAUL
Centre d' Études de Saclay, Orme des Merisiers, F-91191 Gif-sur-Yvette Cedex, France
AND
A. CASTRO-TIRADO[1]
Laboratorio de Astrofísica Espacial y Física Fundamental (LAEFF-INTA), P.O. Box 50727, E-28080 Madrid, Spain
Received 1998 December 7; accepted 1999 December 7

ABSTRACT

Between the launch of the *Ulysses* spacecraft in 1990 October and the entry of *Pioneer Venus Orbiter* (*PVO*) into the atmosphere of Venus in 1992 October, concurrent coverage by *Ulysses*, *PVO*, the WATCH experiments aboard the *Granat* and *Eureca* spacecraft, and the SIGMA and PHEBUS experiments aboard the *Granat* spacecraft was obtained for numerous gamma-ray bursts. Fifteen of them were detected by three or more instruments on spacecraft separated by distances of several AU and could therefore be accurately localized by triangulation. In some cases, independent, accurate locations were obtained by SIGMA and/or WATCH. We present these localizations, which range in area from 0.9 to 530 arcmin^2.

Subject heading: gamma rays: bursts

1. INTRODUCTION

A knowledge of the precise locations of cosmic gamma-ray bursts (GRBs) is important for many studies. When obtained rapidly, they allow multiwavelength counterpart searches to be carried out, which has led to the discovery of fading radio and optical counterparts. After days to months, these fading counterparts are unlikely to be detected, but precise locations, even obtained years later, are useful for statistical studies such as clustering, searches of cataloged objects for possible associations, and host galaxy limits. A number of GRBs have had their redshifts spectroscopically measured or constrained (e.g., Metzger et al. 1997; Kulkarni et al. 1998; Djorgovski et al. 1998), and the results establish a cosmological origin for them, i.e., $z \gtrsim 1$. More recently, however, one burst has been shown to be spatially and temporally coincident with a nearby supernova (Galama et al. 1998), indicating that GRBs may be a diverse phenomenon and that their counterparts may not all be faint galaxies that would be difficult to discern at late times in a relatively large error box. This paper is the fifth in a series presenting GRB localizations by triangulation between spacecraft in the third Interplanetary Network (IPN3), which are separated by several thousand light-seconds. The first two presented results obtained with the *Ulysses*, *Compton Gamma Ray Observatory*, and *Pioneer Venus Orbiter* (*PVO*) or *Mars Observer* spacecraft (Laros et al. 1997, 1998). The third and the fourth are the *Ulysses* supplements to the BATSE 3B and 4Br catalogs (Hurley et al. 1999a, 1999b). This paper presents results obtained with the *Ulysses*, *PVO*, *Granat*, and *Eureca* spacecraft. The *Granat* experiments involved were WATCH, PHEBUS, and/or SIGMA. The *Eureca* experiment was WATCH.

2. INSTRUMENTATION

All of the instrumentation used to obtain the data presented here is based on scintillation crystals, and all the instruments have been described in detail elsewhere. We review each briefly.

The *Ulysses* GRB detector (Hurley et al. 1992) consists of two 3 mm thick hemispherical CsI scintillators with a projected area of about 20 cm^2 in any direction. Its nominal energy range is 25–150 keV. GRB time histories are recorded with time resolutions that range from about 8 ms (in a triggered mode) to 0.5–2 s (in real-time modes). The detector is mounted on a magnetometer boom far from the body of the spacecraft and has a practically unobstructed view of

[1] Instituto de Astrofísica de Andalucía (IAA-CSIC), P.O. Box 03004, E-18080 Granada, Spain.

TABLE 1

BURSTS IN THIS CATALOG

Date	ECT[a]	*Ulysses*	BATSE	*PVO*	WATCH	SIGMA	PHEBUS
1990 Dec 4[b]	09:42:52	Yes[c]	N/O[d]	Yes	Yes	N/O	Yes
1991 Jan 6[e]	16:39:57	Yes	N/O	RI[f]	No[g]	No	Yes
1991 Jan 22	15:13:49	Yes	N/O	Yes	Yes	Yes	Yes
1991 Feb 11.....	03:25:22	Yes	N/O	RI	No	No	Yes
1991 Feb 19[e].....	11:45:24	Yes	N/O	Yes	Yes	No	N/O
1991 Mar 10[b]	13:02:05	Yes	N/O	Yes	Yes	N/O	N/O
1991 Apr 2	14:28:15	RI	N/O	RI	No	Yes	Yes
1991 Apr 17[e].....	20:07:32	Yes	N/O	Yes	No	Yes	Yes
1991 May 17[b].....	05:02:43	RI	No	Yes	Yes[h]	Yes	Yes
1991 Oct 16[b].....	11:01:36	RI	Yes	RI	Yes	N/O	Yes
1991 Oct 18.....	05:32:15	Yes	No	Yes	No	No	Yes
1991 Dec 22	15:00:10	RI	No	RI	No	No	Yes
1992 May 19.....	16:31:53	RI	Yes	Yes	No	N/O	Yes
1992 Jul 14.....	13:04:29	RI	Yes	RI	Yes	Yes	Yes
1992 Jul 23.....	20:03:08	Yes	No	Yes	Yes	Yes	Yes
1992 Oct 4	14:00:21	Yes	No	Yes	Yes	No	N/O

[a] Earth-crossing time, UT.
[b] *Granat* attitude missing.
[c] Burst was observed in a triggered (high time resolution) mode.
[d] Burst was not observable because of, e.g., a data gap, spacecraft not yet launched, etc.
[e] Two possible locations.
[f] Burst was observed in untriggered mode, as a rate increase (low time resolution).
[g] Data were available, clean, and complete, but burst was not observed.
[h] Burst was observed by WATCH, but could not be localized.

the full sky. The *Ulysses* orbit is heliocentric, with a 5 AU aphelion. The instrument has no inherent burst localization capability.

PVO had two burst detectors, consisting of 3.8 cm diameter by 3.2 cm long CsI scintillators, operating in the 100–2000 keV energy range. Time histories were recorded with resolutions ranging from 1/4096 s in time-to-spill mode to 12/1024 s in triggered mode to 16 s in real-time mode. The spacecraft was in orbit around the planet Venus for the observations reported here. Like the *Ulysses* detector, it had no inherent directional capability. Further details may be found in Klebesadel et al. (1980).

The SIGMA telescope was a coded mask-imaging system capable of localizing sources to arcminute accuracy within the fully coded field of view. However, the bursts described in the present paper were observed in the sidelobes, and the

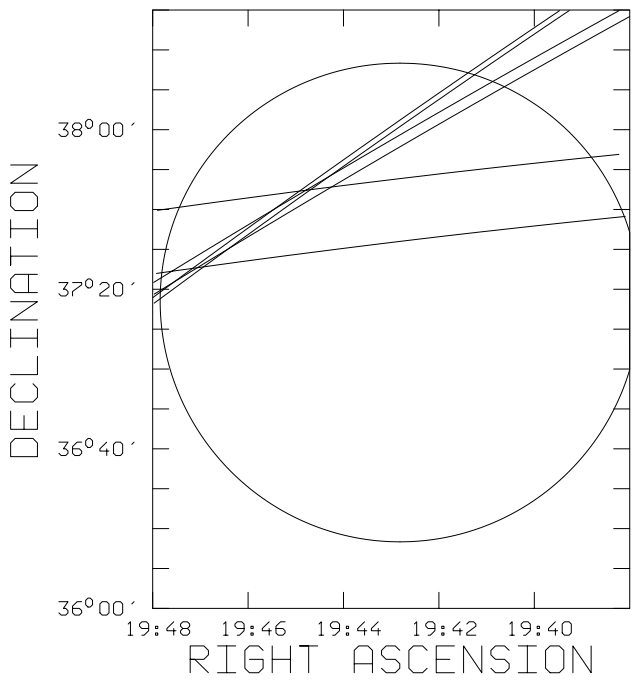

FIG. 1.—IPN3 annuli and WATCH 3 σ error circle for GRB 901204

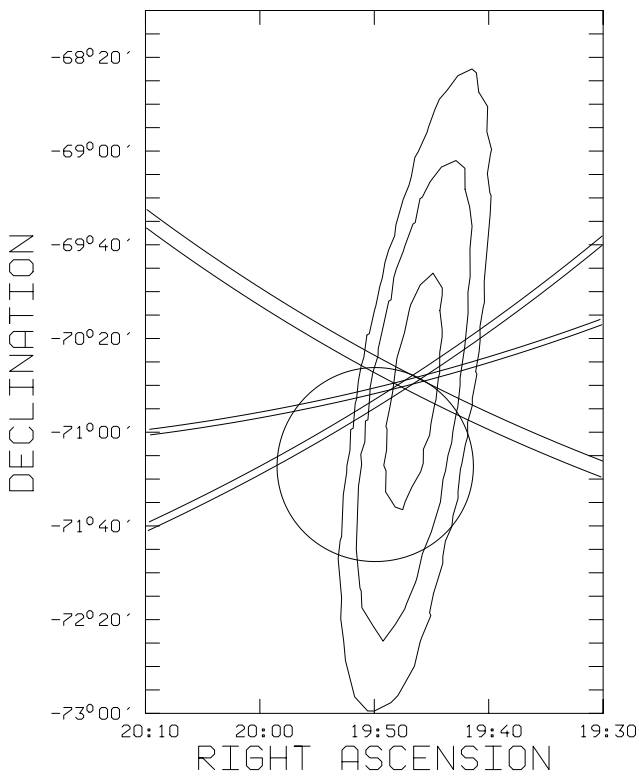

FIG. 2.—IPN3 annuli, WATCH 3 σ error circle, and SIGMA 1, 2, and 3 σ error contours for GRB 910122.

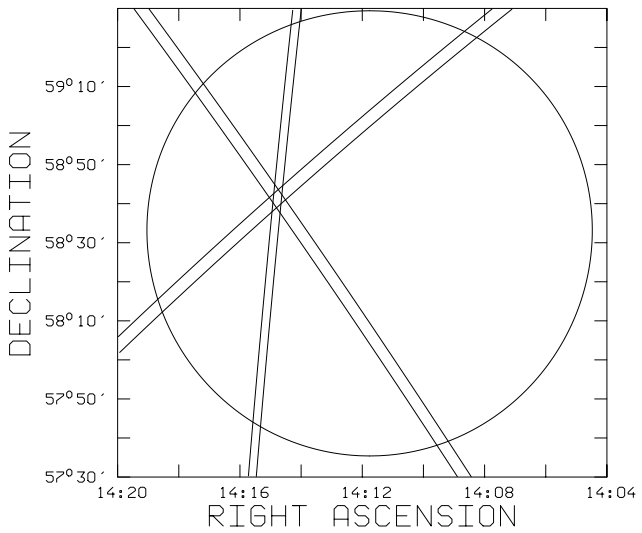

FIG. 3.—IPN3 annuli and WATCH 3 σ error circle for GRB 910219

images were partially coded, leading to accuracies in the tens of arcminutes range and above. The localization procedure is described in Claret et al. (1994). GRB time histories were generally recorded by the SIGMA anticoincidence system, which operated in the energy range above several hundred keV (the precise threshold for any given photon interaction depends on the location of the interaction in the shield). The time resolution was variable, depending on the count rate (time-to-spill mode), but typically was around 100 ms and greater. SIGMA was mounted on the *Granat* spacecraft, which was in a highly eccentric Earth orbit with apogee greater than 70,000 km.

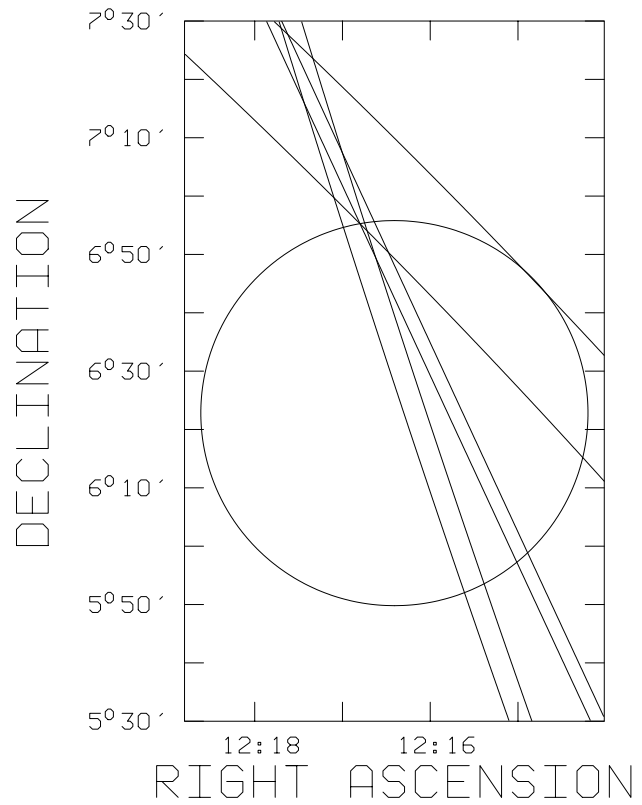

FIG. 4.—IPN3 annuli and WATCH 3 σ error circle for GRB 910310. The major contribution to the WATCH error circle uncertainty in this case is the poorly known *Granat* spacecraft attitude. This systematic error may be underestimated here.

The WATCH instrument was also aboard the *Granat* spacecraft. Based on a novel rotating modulation collimator technique, the WATCH detectors surveyed 80% of the sky and localized bursts to elliptical error boxes, which may be approximated by circles whose 3 σ radii are 0°.2–1°.6. The localization accuracy depends on, among other things, the accuracy with which the attitude of the *Granat* spacecraft can be reconstructed. In general, the spacecraft attitude was derived from the star tracker, which was part of the SIGMA instrument, and when it was operating the uncertainties were negligible as far as the burst locations in this catalog are concerned. However, WATCH detected some bursts at times when SIGMA was off, and only the predicted spacecraft attitude is known. The spacecraft actually oscillates slowly about this predicted position, with peak-to-peak amplitudes of 30′–40′, independently about three axes. In these cases, the attitude was reconstructed by fitting the positions of bright X-ray sources in the WATCH data for periods approximately 30 minutes long about the time of the burst. This procedure recovers the secular drift associated with solar motion, but not the oscillations, and a systematic uncertainty of 0°.5 was assumed to account for them. The energy range was 8–150 keV and the time resolution ranged up to approximately 0.8 s. WATCH/*Granat* is described in Sazonov et al. (1998). A similar instrument was also launched later aboard the *Eureca* spacecraft into low Earth orbit (Lund 1985).

Finally, the PHEBUS experiment was also included in the *Granat* payload (Barat et al. 1988; Terekhov et al. 1991), consisting of six 12 cm long by 7.8 cm diameter BGO detectors oriented along the axes of a Cartesian coordinate system and operating in the 100 keV–100 MeV energy range, with 1/128 to 1/32 s time resolution. By comparing the count rates of the various detectors, it is possible to obtain an approximate source location; the accuracies vary depending on the burst but are in the several tens of degrees range and above. Although quite coarse, this information proved to be very valuable for some of the bursts described here (see below). The spacecraft attitude uncertainties discussed above are negligible compared with the PHEBUS localization uncertainties.

At the time the bursts in this catalog were detected, the interest in providing small error boxes rapidly was recognized. However, the mission designs, in some cases already 15 years old, did not always allow for this. Nevertheless, in three cases (GRB 910219, GRB 911016, and GRB 920714) localizations were done rapidly enough to allow imaging of the fields down to 18th magnitude within three days, although no optical counterparts were found (Castro-Tirado et al. 1994).

3. GRB LOCALIZATION

The precise error boxes presented here have been derived by triangulation, or arrival-time analysis between widely separated spacecraft. ("Widely separated" here means distances of several AU.) This method consists of analyzing the time histories of a GRB as recorded by two spacecraft in order to determine the most likely time difference and its statistical uncertainty. This analysis is done using a χ^2 statistic (e.g., Hurley et al. 1999a; Laros et al. 1997). There is,

TABLE 2

ERROR BOXES OF THE BURSTS IN TABLE 1

DATE	ERROR BOX CORNERS		ERROR BOX CENTER		ERROR BOX AREA (arcmin^2)	MAXIMUM ERROR BOX DIMENSION (arcmin)
	α(2000)	δ(2000)	α(2000)	δ(2000)		
1990 Dec 4[a]	296.197	37.747	296.483	37.586	43	35
	296.766	37.423				
	296.363	37.668				
	296.602	37.503				
	296.173	37.749				
	296.791	37.421				
1991 Jan 22[a]	296.918	−70.681	296.756	−70.646	18	10
	296.595	−70.612				
	296.674	−70.660				
	296.838	−70.633				
	297.000	−70.667				
	296.512	−70.626				
1991 Feb 19[b]	213.731	58.671	213.694	58.688	7.3	4.7
	213.657	58.705				
	213.723	58.710				
	213.665	58.666				
	213.701	58.649				
	213.687	58.727				
1991 Mar 10[b]	184.358	7.266	184.304	7.196	63	38
	184.249	7.125				
	184.198	6.921				
	184.405	7.462				
	184.424	7.480				
	184.178	6.901				
1991 Apr 2[a]	77.612	13.611	77.629	13.690	35	14
	77.647	13.768				
	77.598	13.675				
	77.661	13.704				
	77.631	13.571				
	77.627	13.810				
1991 May 17[a]	150.475	−42.876	150.602	−42.780	236	92
	150.730	−42.693				
	149.659	−43.107				
	151.546	−42.447				
	151.545	−42.447				
	149.659	−43.107				
1991 Oct 16[c]	297.996	−5.386	298.137	−4.811	530	70
	298.151	−4.220				
	298.148	−5.205				
	298.251	−4.434				
1991 Oct 18[a]	5.468	31.957	6.009	31.658	50	74
	6.542	31.353				
	5.401	31.992				
	6.608	31.316				
	6.486	31.397				
	5.526	31.914				
1991 Dec 22[a]	87.139	13.137	87.084	14.062	200	118
	87.005	14.938				
	87.159	13.274				
	87.023	15.111				
1992 May 19[a]	321.422	44.221	321.254	44.137	21	23
	321.485	44.228				
	321.024	44.046				
	320.087	44.053				
1992 Jul 14[d]	220.826	−30.721	220.857	−30.610	36	20
	220.897	−30.506				
	220.848	−30.607				
1992 Jul 23[a]	287.128	27.216	287.142	27.232	0.9	3.2
	287.155	27.248				
	287.126	27.210				
	287.157	27.255				
	287.148	27.249				
	287.135	27.215				

TABLE 2—*Continued*

Date	Error Box Corners α(2000)	Error Box Corners δ(2000)	Error Box Center α(2000)	Error Box Center δ(2000)	Error Box Area (arcmin²)	Maximum Error Box Dimension (arcmin)
1992 Oct 4[e].....	219.244	34.180	219.236	34.180	3.25	8.25
	219.261	34.115				
	219.211	34.246				
	219.228	34.180				

[a] *Ulysses*/PHEBUS/*PVO* triangulation error box.
[b] *Ulysses*/*PVO*/WATCH triangulation error box.
[c] *Ulysses*/BATSE and*Ulysses*/*PVO* annuli intersect at grazing incidence; error box is defined by the four intersections of the*Ulysses*/BATSE annulus and the WATCH error circle.
[d] *Ulysses*/BATSE and*Ulysses*/*PVO* annuli intersect at grazing incidence; the annuli in turn graze the WATCH error circle. The error box is defined by the three intersections of the*Ulysses*/BATSE annulus and the WATCH error circle.
[e] *Ulysses*/*PVO*/WATCH triangulation error box.

however, an important difference between the events presented here and those presented in previous catalogs, which requires further explanation.

GRB time histories are energy-dependent. A time history taken in the 25–100 keV *Ulysses* energy range may differ from that taken in the *PVO* 100–2000 keV range. The magnitude of this difference varies considerably from event to event and can easily be judged in, say, the χ^2 technique (Hurley et al. 1999a), where the goodness of fit is reflected in the value of χ^2 per degree of freedom. When the "fit" between two time histories is poor, the estimate of the statistical uncertainty in the time difference may become unreliable. This, in turn, renders the annulus width estimates, and hence the confidence value for the error box, suspect. In previous GRB location catalogs, we have been able to avoid this problem by comparing time histories in the same or very similar energy ranges. Thus, in the *Ulysses*/BATSE catalogs, 25–150 keV *Ulysses* time histories were compared with 25–100 keV BATSE time histories, and the fits were generally satisfactory (Hurley et al. 1999a, 1999b). In the *Ulysses*/BATSE/*PVO* catalog, the 25–150 *Ulysses* time histories were again compared with the 25–100 keV BATSE time histories, but the 100–2000 keV *PVO* time histories were compared with the BATSE time histories greater than 100 keV.

In the present catalog, we have four instruments—*Ulysses*, *PVO*, PHEBUS, and SIGMA—which recorded their time histories in a single energy range that was different from all the others. Some of these energy ranges, e.g., *Ulysses*'s and SIGMA's, do not even overlap. We have therefore used the following techniques to assure that the error boxes are conservatively estimated. First, we have used the PHEBUS 100 keV–100 MeV time history for the comparisons instead of the SIGMA one (every SIGMA event in this catalog was also observed by PHEBUS). Second, we perform the following internal consistency check.

Let δT_{i-j} be the difference in arrival times between spacecraft i and spacecraft j. Let the subscript c denote the calculated values, and t the true values, unknown to the

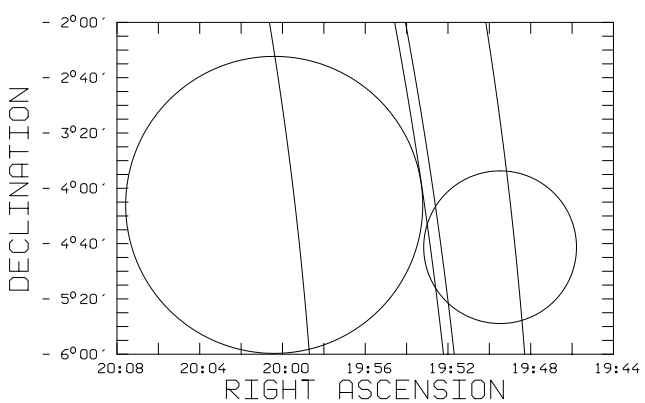

FIG. 5.—BATSE 1 σ error circle (*left*; Meegan et al. 1996), WATCH 3 σ error circle (*right*), and IPN3 annuli for GRB 911016. The narrow annulus is fully contained within the wider one; its intersection with the WATCH error circle defines the error box.

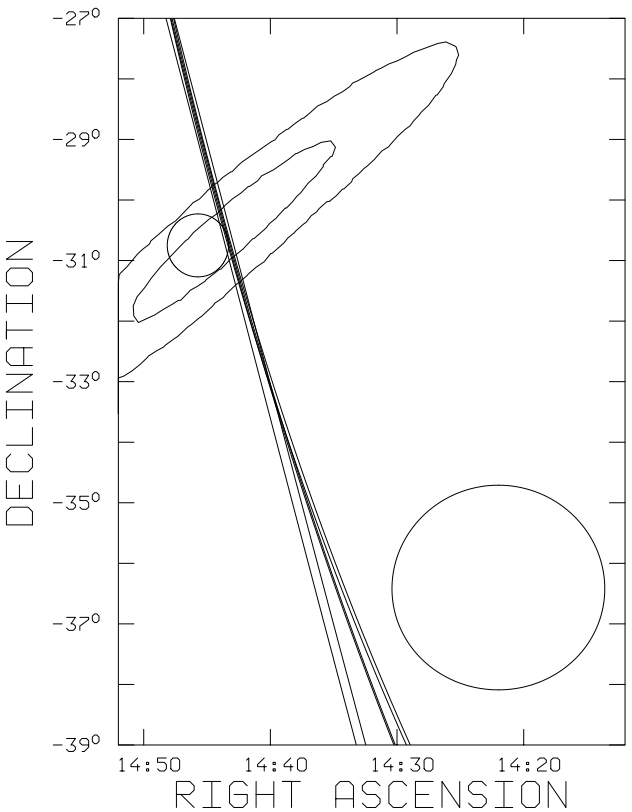

FIG. 6.—BATSE 1 σ error circle (*bottom right*; Meegan et al. 1996), WATCH 3 σ error circle (*top left*), IPN3 annuli (intersecting at grazing incidence), and SIGMA 1 and 2 σ error contours for GRB 920714. The major contribution to the WATCH error circle uncertainty in this case is the poorly known *Granat* spacecraft attitude. The systematic error may be underestimated here.

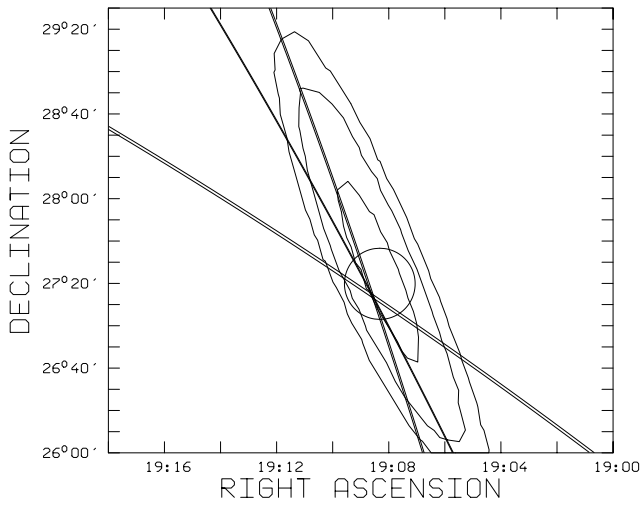

FIG. 7.—WATCH 3 σ error circle, SIGMA 1, 2, and 3 σ error contours, and IPN3 annuli for GRB 920723.

experimenter. Then, for a network of three spacecraft, $\delta T_{1-2,t} + \delta T_{1-3,t} + \delta T_{3-2,t} \equiv 0$. In general, the sum of the calculated values will not be zero, because of a combination of statistical and systematic errors: $\Delta \equiv \delta T_{1-2,c} + \delta T_{1-3,c} + \delta T_{3-2,c} \neq 0$. Let $\sigma(\delta T_{i-j})$ be the statistical error associated with $\delta T_{i-j,c}$. (We have shown in Hurley et al. 1999a that the error distribution should be approximately normal). In those cases where Δ is incompatible with the values of $\sigma(\delta T_{i-j})$, we increase them appropriately.

Finally, we note that the events in this catalog were all observed by just three widely separated spacecraft. Triangulation therefore yields two possible intersection points for the annuli. We have generally used the localization capabilities of WATCH and SIGMA to identify the correct intersection. In those cases where no WATCH or SIGMA data were available, we have used the PHEBUS location capability to identify the intersection.

4. GRB LOCATIONS

Table 1 gives the dates and times of the bursts and identifies the spacecraft that observed them and their operating modes. In some cases, bursts were observed by additional near-Earth spacecraft, such as the U.S. Air Force *Defense Meteorological Satellite Program* (*DMSP*; Terrell et al. 1998). These data were consistent with those of other near-Earth spacecraft, however, and their use did not constrain the error boxes further. Also, some events were localized to two alternate error boxes that could not be distinguished using the directional response of any of the instruments. These are not discussed further.[2] This table also indicates which bursts were observed when the SIGMA star tracker was off and the spacecraft attitude could not be precisely determined, as discussed above.

For the bursts in Table 1, Table 2 gives the corners of the 3 σ confidence error box, the center of the error box, its area, and its maximum dimension. The epoch for the coordinates is J2000. In general, the smallest possible error box derived from triangulation using three spacecraft will be defined by four or six corners from the intersection of three annuli (depending on the width of the annuli), but in some cases, as noted in Table 2 and the figure legends, grazing intersections may reduce this number. The coordinates have been corrected to the heliocentric frame (the equivalent of the aberration correction—see Hurley et al. 1999a) and supersede all previous data on these bursts. Some of the error boxes are shown in Figures 1, 2, 3, 4, 5, 6, and 7. In two cases the WATCH and IPN3 annuli are only marginally compatible (Figs. 4 and 6); it is thought that the cause is (1) the imprecisely known *Granat* spacecraft attitude, which may result in a systematic underestimate of the total WATCH error circle radius, and/or (2) the approximation of the elliptical WATCH locations by circles.

5. CONCLUSIONS

IPN3 error box areas are comparable in size to, or in some cases much smaller than, those that can be derived rapidly from wide-field X-ray cameras such as the one on board *BeppoSAX* ($\approx 10'$ error circle radius—e.g., Costa et al. 1997). For most of the events in this catalog, the initial error boxes were circulated to the astronomical community with delays that were considerably greater than those that can be achieved by *BeppoSAX*. However, the fact that fading optical transients can be detected in the *BeppoSAX* wide-field camera error circles even several days after the burst means that an IPN that can deliver small error boxes on $\approx$ day timescales will be useful for counterpart identifications. Such a network now exists, consisting of *Ulysses*, BATSE, and the *Near Earth Asteroid Rendezvous* mission (Cline et al. 1999).

Finally, we note that over 50 bursts were detected by *Ulysses*, WATCH, and in some cases other spacecraft, which provide error boxes with areas of several hundred arcmin^2. Publication of these events is in progress (Hurley et al. 2000).

K. H. is grateful to JPL Contract 958056 for *Ulysses* operations.

[2] Full details of these events in particular, and all bursts in general, localized by the IPN3, may be found at http://ssl.berkeley.edu/ipn3/index.html.

REFERENCES

Barat, C., et al. 1988, in AIP Conf. Proc. 170, Nuclear Spectroscopy of Astrophysical Sources, ed. N. Gehrels & G. Share (New York: AIP), 395
Castro-Tirado, A., Brandt, S., Lund, N., & Guziy, S. 1994, in AIP Conf. Proc. 307, 2d Workshop on Gamma-Ray Bursts, ed. G. Fishman, J. Brainerd, & K. Hurley (New York: AIP), 404
Claret, A., et al. 1994, A&A, 287, 824
Cline, T., et al. 1999, A&AS, 138, 557
Costa, E., et al. 1997, Nature, 387, 783
Djorgovski, S., et al. 1998, GCN Circ. 137 (http://gcn.gsfc.nasa.gov/gcn/gcn3/137.gcn3)
Galama, T., et al. 1998, Nature, 395, 670
Hurley, K., et al. 1992, A&AS, 92, 401
———. 1999a, ApJS, 120, 399
———. 1999b, ApJS, 122, 497
Hurley, K., et al. 2000, ApJS (in press)
Klebesadel, R., Evans, W., Glore, J., Spalding, R., & Wymer, F. 1980, Proc. IEEE, 18, 76
Kulkarni, S., et al. 1998, Nature, 393, 35
Laros, J., et al. 1997, ApJS, 110, 157
Laros, J., et al. 1998, ApJS, 118, 391
Lund, N. 1985, Proc. SPIE, 597, 95
Meegan, C., et al. 1996, ApJS, 106, 45
Metzger, M., et al. 1997, Nature, 387, 878
Sazonov, S., et al. 1998, A&AS, 129, 1
Terekhov, O., et al. 1991, Adv. Space Res., 11(8), 129
Terrell, J., Lee, P., Klebesadel, R., & Griffee, J. 1998, in AIP Conf. Proc. 428, 4th Huntsville Symp. on Gamma-Ray Bursts, ed. C. Meegan, R. Preece, & T. Koshut (New York: AIP), 54